The International Journal of Advanced Manufacturing Technology (2018) 97:209–228
https://doi.org/10.1007/s00170-018-1936-7

ORIGINAL ARTICLE

Temperature field model and experimental verification on cryogenic air nanofluid minimum quantity lubrication grinding

Jianchao Zhang[1] · Changhe Li[1] · Yanbin Zhang[1] · Min Yang[1] · Dongzhou Jia[1] · Yali Hou[1] · Runze Li[2]

Received: 27 November 2017 / Accepted: 19 March 2018 / Published online: 28 March 2018

Abstract

Considering the poor lubricating effect of cryogenic air (CA) and inadequate cooling ability of nanofluid minimum quantity lubrication (NMQL), this work proposes a new manufacturing technique cryogenic air nanofluid minimum quantity lubrication (CNMQL). A heat transfer coefficient and a finite difference model under different grinding conditions were established based on the theory of boiling heat transfer and conduction. The temperature field in the grinding zone under different cooling conditions was simulated. Results showed that CNMQL exerts the optimal cooling effect, followed by CA and NMQL. On the basis of model simulation, experimental verification of the surface grinding temperature field under cooling conditions of CA, MQL, and CNMQL was conducted with Ti–6Al–4V as the workpiece material. Simultaneously, CNMQL exhibits the smallest specific tangential and normal grinding forces (2.17 and 2.66 N/mm, respectively). Further, the lowest grinding temperature (155.9 °C) was also obtained, which verified the excellent cooling and heat transfer capabilities of CNMQL grinding. Furthermore, the experimental results were in agreement with theoretical analysis, thereby validating the accuracy of the theoretical model.

Keywords Grinding · Cryogenic air · Nanofluid minimum quantity lubrication · Finite difference simulation · Heat transfer coefficient · Temperature field · Boiling heat transfer

1. On the basis of theory of boiling heat transfer and conduction, a heat transfer coefficient model and a finite difference model under different grinding conditions were established, and the temperature field in the grinding zone under different cooling conditions was simulated.
2. The experimental verification of the surface grinding temperature field under cooling conditions of CA, MQL, and CNMQL was carried out.
3. Al_2O_3 nanoparticles was added to synthesis lipid to prepare nanofluids, and workpiece material Ti-6Al-4V was studied.
4. Numerical simulation and experimental results were discussed.
5. The cooling performance and heat transfer mechanism under different cooling conditions were analyzed.

✉ Changhe Li
sy_lichanghe@163.com

Jianchao Zhang
17863902108@163.com

Yanbin Zhang
zhangyanbin1_qdlg@163.com

Min Yang
yummy0lige@163.com

Dongzhou Jia
jia_dongzhou@163.com

Yali Hou
510601951@qq.com

Runze Li
runzeli@usc.edu

[1] School of Mechanical Engineering, Qingdao University of Technology, Qingdao 266520, China

[2] Department of Biomedical Engineering, University of Southern California, Los Angeles, CA 90089-1111, USA

Nomenclature

CA	cryogenic air
MQL	minimum quantity lubrication
NMQL	nanofluids minimum quantity lubrication
CNMQL	cryogenic air nanofluids minimum quantity lubrication
V_s	peripheral velocity of grinding wheel (m/s)
V_w	feed speed (mm/min)
a_p	cutting depth (μm)
a	nozzle angle (°)
P	gas pressure (MPa)
F'_t	specific tangential grinding force (N/mm)
F'_n	specific normal grinding force (N/mm)
F_t	tangential grinding force (N)
F_n	normal grinding force (N)
b	grinding width (mm)
α	thermal diffusion coefficient (m^2/s)
T	transient temperature (°C)
t	total grinding time (s)
ρ_w	density of workpiece (kg/m^3)
c_w	specific heat capacity of workpiece (J/[kg·K])
q_{total}	total heat flux density (J/[m^2·K·s])
Q	grinding power (J/s)
S	contact area (mm^2)
l_c	contact arc (mm)
d_s	grinding wheel diameter (mm)
a_p	grinding depth (μm)
R	energy ratio coefficient
q_w	heat flux density transmitted into the workpiece (J/[m^2·K·s])
k	thermal conductivity coefficient (W/[m^2·K])
β	a constant
θ_{max}	peak temperature rise (°C)
ΔT	temperature difference (°C)
ΔT_s	the minimum degree of superheat to produce bubbles (°C)
σ	surface tension (N/m)
T_s	boiling point of liquid (°C)
r	radius (mm)
p_l	density of liquid (kg/m^3)
p_g	air density (kg/m^3)
μ_l	dynamic viscosity of liquids (cP)
Nu	Nusselt number
ΔT_{min}	the minimum degree of film boiling heat transfer (°C)
p'_g	gas film density (kg/m^3)
K'_g	air film heat transfer coefficient (kJ/[m·K·s])
ζ	latent heat (kJ/kg)
h_a	convection heat transfer coefficient (W/[m^2·K])
λ_a	thermal conductivity of air (W/[m^2·K])
l	heat transfer width (mm)
μ_a	gas dynamic viscosity (cP)
c_a	air pressure specific heat capacity (J/[kg·K])
Q'	supply amount of nanofluids per unit grinding time ($\mu m^3/s$)
r_{surf}	pavement radius of single droplet (μm)
N_l	quantity of droplets
a	length of the workpiece (μm)
V_l	volume of a single droplet (μm^3)
d_0	spherical diameter of a single droplet (μm)
θ	contact angle (°)
c_l	specific heat capacity of droplets (J/[kg·K])
h_{n1}	convective heat transfer coefficient of in natural–convection heat transfer (W/[m^2·K])
h'_a	convective heat transfer coefficient of room temperature air (W/[m^2·K])
h_{n2}	convective heat transfer coefficient of initial point of the transition boiling heat transfer (W/[m^2·K])
q'_a	convection heat transfer of air at room temperature (J/[m^2·K·s])
h_{fa}	latent heat of vaporization (kJ/kg)
T_{n2}	starting point temperature of transition boiling heat transfer (K)
T_l	temperature of nanofluids (K)
p_a	internal pressure in the nozzle (Pa)
p_o	barometric pressure (Pa)
v_l	effluent velocity of droplets (m/s)
v_n	vertical velocity (m/s)
λ_v	thermal conductivity of steam (W/[m·K])
μ_v	steam viscosity (cP)
c_v	thermal capacity of mass (J/[kg·K])
h_{n3}	convective heat transfer coefficient at the initial point of film boiling (W/[m^2·K])
Δt	time increment
O	infinitesimal quantity
G	comprehensive coefficient of heat transfer (W/[m^2·K])
U_1	internal energies of phase 1
V1	volume of unit mass
h1	entropies per unit mass of phase 1

1 Introduction

Grinding is widely used in various fields because of its high processing accuracy, strong technological adaptability, and applicability to many materials. This process plays an important role in advanced manufacturing technologies. During grinding, relatively high-speed motion and friction, plowing, and cutting between abrasive particles and workpieces will consume abundant energy. Meanwhile, grinding consumes higher amounts of energy to remove a unit volume of materials compared with other processing techniques because grinding particles generally have negative rake [1]. Energy generated during grinding is mainly converted into heat. Concentrated heat forms a local high-temperature region in

the grinding zone, thereby causing certain surface heat damages in materials, such as surface oxidization, burning, and even cracks and residual stress. These damages will deteriorate the surface quality of workpiece. High temperature may intensify the wear of the grinding wheel and deteriorate fatigue resistance, leading to shortened processing accuracy and service life of the grinding wheel [2–5]. Thus, the processes of effectively cooling and lubricating the grinding zone are of great significance.

During grinding, high-speed rotation of the grinding wheel will drive the movement of surrounding air, forming a dense air barrier layer surrounding the grinding wheel. Only 5 to 40% of the grinding fluids reach the grinding contact zone for cooling and lubricating due to the hindrance by the air barrier layer [6–8]. The use of abundant cutting fluids results in resource waste and environmental pollution. Traditional pouring lubrication cannot adapt to the requirements of environment-friendly production. Scholars have conducted many explorations and studies and proposed minimum quantity lubrication (MQL). In this process, a minimum quantity of grinding fluids (generally, grinding fluids dosage per unit of grinding wheel width is 0.03–0.2 L/h) is mixed into high-pressure air (0.4–0.65 MPa), atomized under the assistance of high-pressure air flow, and injected into the high-temperature grinding zone for cooling and lubricating [4]. Assisted by high-pressure air, grinding fluids can break the air barrier layer at a high speed and strong impact and then enter into the grinding interface, thereby enabling the fluids to reach the grinding zone. One lubricating film layer will be formed by adsorbing lubricating oil into the grinding wheel/workpiece contact surface, which can offer effective lubricating performance. High-pressure air continuously scours the surface at a high speed. This phenomenon cannot only eliminate abrasive debris but can also realize forced-convection heat transfer on the workpiece surface and reduce grinding temperature in the grinding zone to achieve good cooling effect. Basing on the development of nanotechnology and theory of solid heat transfer enhancement [8], some scholars added solid nanoparticles into the minimum quantity fluids and proposed nanofluid minimum quantity lubrication (NMQL) based on MQL. NMQL possesses excellent thermal conductivity and tribological property. Under the same volume content, the surface area and heat capacity of nanoparticles are higher than those of solid particles with size ranging from millimeter to micrometer level. Thus, the thermal conductivity of nanofluids sharply increases. The addition of nanofluids can increase the heat exchange performance of lubricating fluids; this process can also enhance heat exchange and decrease the temperature in the grinding zone [9–11]. Nanofluids possess excellent properties of antiwear, anti-friction, and high-bearing capacity, which enhance the tribological properties of lubricating fluids. Except for the inherent advantages of MQL grinding, NMQL significantly improves the cooling and lubricating performance, reduces the grinding force and the occurrence of grinding-induced burning damages, improves the processing quality of workpieces, and prolongs the service life of the grinding wheel [12, 13]. Therefore, NMQL is a new environment-friendly, resource-saving, and high-energy utilization of sustainable lubrication model. Luo et al. [14] studied the lubricating properties of Al_2O_3 nanoparticles as lubricating oil additives by four-ball and thrust-ring friction tests; the results discovered that the friction coefficient and the wear scar diameter are the smallest when the added concentration is 0.1 wt%. The lubrication mechanism is the formation of a self-laminating protective film on the friction surface, and the wear behavior changes from sliding friction to rolling friction. Mao et al. [15] performed an experimental study on the Al_2O_3 NMQL grinding of AISI 52100 steel. Compared with MQL, NMQL grinding can significantly reduce the grinding force, grinding temperature, and surface roughness, indicating its improved surface processing quality. Mao et al. also studied the effect of NMQL parameters and found that the lowest grinding temperature was achieved at the 15° nozzle angle, 20 mm distance between the nozzle and the grinding zone, and 0.6 MPa air pressure [16]. Zhang et al. [17] used soybean, palm, and rapeseed oils as base oils to evaluate the grinding and lubricating properties of MQL with nanoparticles under the following four grinding working conditions: dry grinding, flood grinding, MQL (using three vegetable oils and liquid paraffin), and NMQL (using nanoparticles of different concentrations). Palm oil-based nanofluids with MoS_2 exhibit the optimal lubricating property under NMQL condition because of the high fatty acid content and film-forming property of carboxyl in palm oil. Anuj et al. [18] mixed Al_2O_3 nanoparticles in conventional cutting fluids at different concentrations and examined their machining performance in turning of AISI 1040 steel through MQL technique. The experimental results clearly revealed that the performance of Al_2O_3 nanofluids in terms of surface roughness, tool wear, cutting force, and chip morphology was better compared with dry machining, wet machining with conventional cutting fluid, and MQL using conventional cutting fluid. Guo et al. [3] mixed castor oil with six kinds of vegetable oils at a ratio of 1:1 for minimum quantity lubrication (MQL) grinding and evaluated the lubricating performance. The comprehensive lubricating performance of mixed oil is superior to that of castor oil, and soybean/castor oil exhibits the optimal performance. The specific tangential and normal grinding forces are 27.03 and 23.15% reduction, respectively, with respect to those of castor oil. Lee et al. [19] added nanodiamond and Al_2O_3 nanoparticles into paraffin oil with nanofluid MQL microgrinding. The nanofluid MQL is effective for reducing grinding forces and enhancing surface quality. The authors also discovered that the type, size, and volumetric concentration of the nanoparticles are critical parameters that influence the properties of microgrinding process. Hadad et al. [20]

conducted an experimental study on the grinding temperature and energy distribution of MQL grinding of brittle hard 100Cr6 steel by using aluminum oxide grinding and CBN grinding wheels. The results found that the CBN grinding wheel can improve the shortcomings of MQL cooling. Setti et al. [21] applied Al_2O_3 nanofluids in the grinding of Ti alloy and found that the Al_2O_3 nanofluids can reduce the grinding force and surface quality of processing workpiece. Su et al. [22] investigated the turning effect of NMQL with vegetable-based and ester oils as base fluids under different cooling conditions. The experimental results showed that application of graphite oil-based NMQL significantly reduced the cutting force and temperature than that under other cooling conditions.

Researchers proposed cryogenic air (CA) to effectively reduce the grinding temperature in the grinding zone and decrease the grinding-induced burning damages. In this processing technique, the cooling medium is cooled to about 0 to 30 °C by the cooling equipment and then sprayed to the processing region by nozzle for cooling and lubrication. The cooling medium mainly includes cold air, liquid nitrogen, and argon [23]. Compared with traditional dry grinding, CA achieves significantly lower temperature in the grinding zone and friction force between the grinding wheel and workpiece. Simultaneously, CA prolongs the service life of the grinding wheel, protects the sharpness of the abrasive particles, and increases the workpiece surface quality. Compared with traditional cooling lubricating modes, CA can increase the processing efficiency and workpiece surface quality; CA also has high availability of the cooling medium (e.g., air) and is environment friendly. Simultaneously, CA can reduce the production cost and conform to the philosophy of environment-friendly processing.

Manimaran et al. [24] reported that applying LN_2 reduces the grinding force by up to 32%, improves Ra by 30 to 49%, and reduces the grinding zone temperature within the range of 45–49%. Ravi et al. [25] presented the experimental investigations of the influence of cryogenic cooling by LN_2 jet on the milling performance of the hardened AISI D3 tool steel. The experimental results revealed that the cutting temperatures are reduced by 43–48% and 26–35%, and the mean cutting forces are decreased by 40–50% and 22–39% in dry and wet machining, respectively. Jawahir et al. [26] investigated the comprehensive effects of cryogenic cooling on the drilling performance and surface integrity characteristics of the CFRP composite material. The findings demonstrated that cryogenic cooling has a profound effect on reducing the cutting edge rounding of the drill bit and outer corner wear; it also helps to enhance the surface integrity characteristics of the produced hole. Paul et al. [27] reported that cryogenic coolant reduces tensile residual stress for all materials under different feed levels. Simultaneously, cryogenic coolant exhibits better chip formation, lesser grinding force, and lower grinding zone temperature compared with an oil-based coolant. Hence, LN_2 application is effective in controlling the grinding force, Ra, and grinding zone temperature. Schoop et al. [28] have discussed the differences in chip morphology, cutting temperature, and surface quality under cooling conditions of CA, MQL, and dry cutting. Experimental results demonstrated that CA can reduce flank wear of the cutting tools and decrease temperature better than MQL and dry cutting. MQL can obtain the lowest cutting force and best chip morphology and surface quality. Adopting CA during high-speed cutting will reduce temperature in the cutting region, while using MQL during low-speed cutting will achieve better lubricating effect. Su et al. [29] compared cutting force, cutting temperature, and tool wear during high-speed turning of Ti alloy under dry cutting, room-temperature high-speed air cutting, MQL, CA, and CAMQL cutting. Results demonstrated that CAMQL can not only reduce temperature in the cutting zone more effectively than MQL grinding under normal temperature, but also possess outstanding lubricating advantages, weaken cutting force and prolong service life of cutting tools.

NMQL has good lubricating performance, but it has poor heat transfer effect of compressed air under room temperature. Although CA can reduce the temperature effectively, it has poor lubricating performance due to the lack of lubricating medium. Considering that these two green processing technologies have some shortages in actual applications, NMQL and CA are combined; thus, cryogenic air nanofluid minimum quantity lubrication (CNMQL) was proposed. Cryogenic air carries nanolubricating fluids to play the role of cooling and lubricating in the grinding zone. Cryogenic air can eliminate debris and cool the grinding zone. Meanwhile, it lowers temperature on the processing material surface and improves processing performance of the materials. On the other hand, a substantial temperature gap can be observed between the produced cryogenic air flow and the grinding zone, which can intensify the heat transfer effect. One lubricating film layer, which is formed by the minimum nanolubricating fluids on the workpiece surface, can cool and lubricate the processing zone, as well as reduce the friction force and heat generation between the grinding wheel and workpiece, thereby realizing excellent cooling effect. This technique can not only increase the processing quality and efficiency, but it can also avoid environmental pollution and damages to workers; it also has low cost and meets the requirements of green manufacturing and sustainable development. Li et al. [30] have mixed minimal quantity of cutting fluids into LN_2 for milling of the Ti alloy; they have also discussed the effects of room temperature nitrogen oil and pure LN_2 and LN_2 oil mixture media. Research demonstrated that compared with the two other working conditions, LN_2 oil mixture medium has better lubricating performance and significantly lower milling force. On the basis of the analysis of the tool wear form, researchers have disclosed the tool wear mechanism under three working conditions. He et al. [31] performed

experiment on 304 stainless steel with cutting tool under cutting conditions of CA, CAMQL, and dry cutting. Experimental results demonstrated that CAMQL can effectively reduce the surface roughness and improve the chip-breaking ability and durability of cemented carbide tool. Wang et al. [32] have performed an experiment to explore the grinding performance of TC4 under the conditions of CA, LN_2, flood cooling, and CAMQL. The experimental results indicated that CAMQL can not only improve metal removal rate and the life of belt, but it can also effectively reduce the grinding temperature.

On the basis of the literature review above, we concluded that although scholars have conducted impressive explorations of CA and MQL in all kinds of mechanical machining processes, only few researches have studied on the grinding performance under CNMQL condition. In this study, the grinding experiment of Ti–6Al–4V under different cooling conditions was conducted. Moreover, the heat exchange mechanism of CNMQL was discussed through numerical simulation and experiment.

2 Experiment

2.1 Experimental setup

The experiment was conducted using a K–P36 numerical control precision surface grinder. The main technological parameters of the surface grinder are presented in Table 1. The grinder was equipped with a magnetic workbench; the working range was 600 × 300 mm, and the size was 950 × 1000 mm. The nanofluids transfer device called Bluebe minimum quantity oil supply system was used. The VC62015G vortex tube was adopted as the cryogenic air cooling equipment. During the data collection, the grinding forces were measured online using the piezoelectric dynamometer (YDM–III99) that was attached with multichannel charge amplifier and was run with a software. The thermocouple method was used to measure the temperature. The surface morphology of the workpiece was observed using scanning electron microscope.

Table 1 Parameters of K–P36 numerical control precision surface grinder

Machine parameters	Value
Principal axis power	4.5 kW
Highest rotating speed of spindle	4800 rev/min
Wheel size	300 mm × 20 mm × 76.2 mm
Wheel particle size	160 mesh
Highest peripheral velocity of grinding wheel	50 m/s

The experimental equipment and sequence visualization are shown in Fig. 1.

2.2 Experimental materials

In the experiment, Ti–6Al–4V was used as the workpiece material. Ti alloy is increasingly used in aviation, aerospace, navigation, and other industrial departments because of its excellent mechanical properties, such as high hardness, high strength, high thermal stability, strong corrosion resistance, and high reserves. Ti alloy is also a material that is difficult to be processed and will generate high temperature and stress, resulting in difficult processing, poor surface quality of products, and short service life of the cutting tools. Therefore, experimental studies on Ti–6Al–4V grinding have significance. Workpiece size is 40 mm × 30 mm × 30 mm. The chemical composition and performance parameters of the workpiece are listed in Tables 2 and 3.

In this experiment, the KS–1008 synthesis lipid was used to prepare 2% volume fraction of the Al_2O_3 nanofluids using the following steps [22]. First, the Al_2O_3 nanoparticles were added into the KS–1008 synthesis lipid according to the volume fraction of 2%. Afterward, 0.1% volume fraction of the dispersing agent, which is 12 units of sodium alkyl sulfate (SDS), was added. The Al_2O_3 nanofluids with a volume fraction of 2% have good lubricating and tribological properties [33]. Nanoparticles are unstable and easy to agglomerate in the base oils. Thus, adding a small amount of surfactants in nanofluids can improve its stability. Dema et al. [34] found that the addition of a small amount of SDS has little effect on the tribological properties, but it has considerable effect on the dispersion and stability of the nanoparticles. Second, they were stirred by machines and vibrated in the ultrasonic oscillator for 2 h to prepare nanofluids with high dispersing performance and suspension stability. The physical properties of the Al_2O_3 nanoparticles are shown in Table 4.

2.3 Experimental conditions

In this experiment, Ti–6Al–4V was used as the workpiece material during plane grinding to explore the cooling and heat transfer performances under three different cooling conditions, namely, CA, MQL, and CNMQL.

The carbide ceramic-bonded SiC grinding wheel was adopted in the experiment, and the specific model is GC80K12V. The uniform experimental grinding process parameters in the experiment are shown in Table 5. Temperature and air flow at the nozzle outlet under three cooling conditions in the experiment are shown in Table 6.

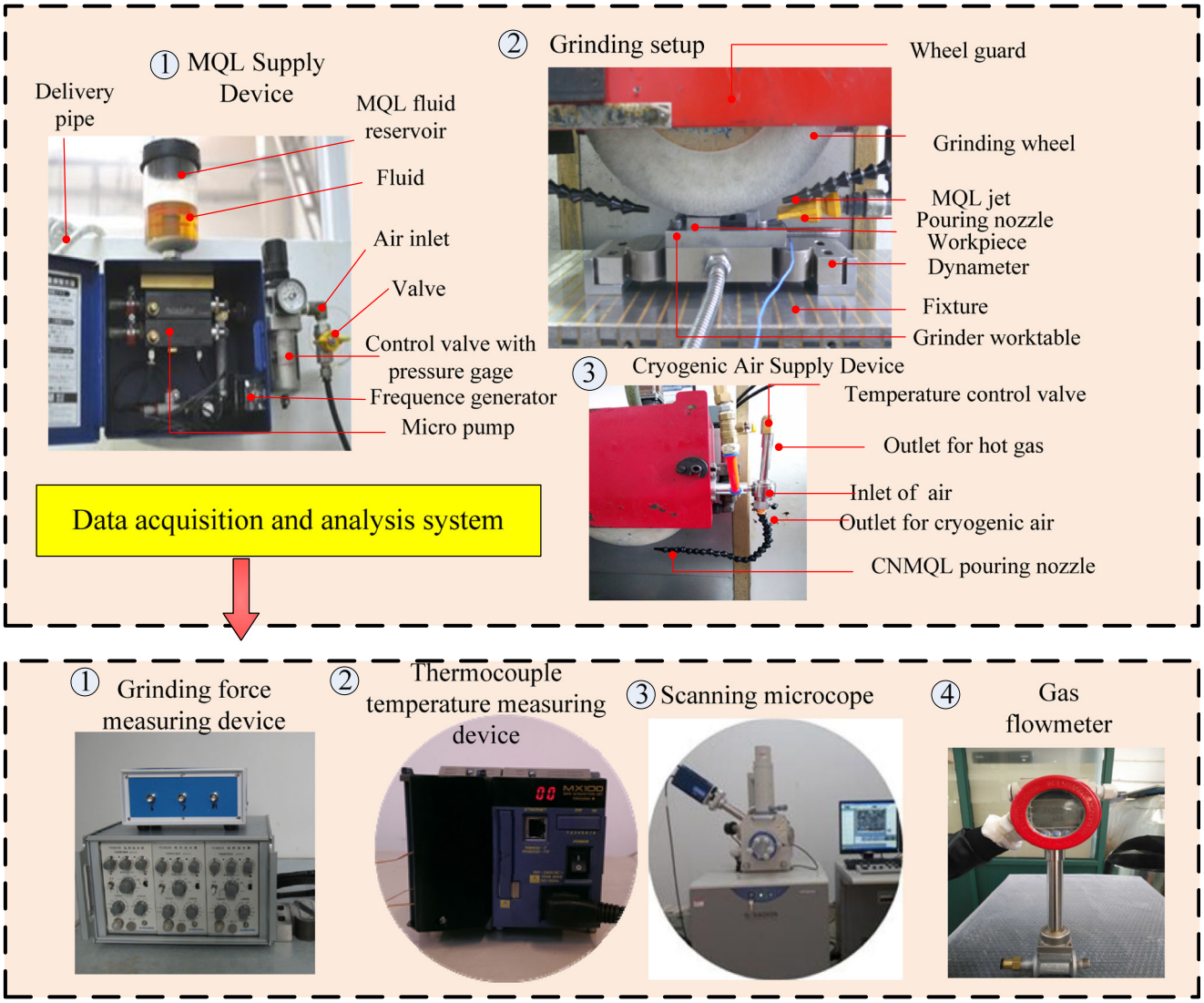

Fig. 1 Experimental equipment and sequence visualization

The grinding wheel was finished before every experiment to achieve controllable grinding process and same conditions for every grinding experiment. The dressing parameters of the grinding wheel are listed in Table 7.

For each experiment, a 3D grinding force dynamometer was used to measure and record the normal, tangential, and axial forces. The measured sample frequency of the grinding force was 1 kHz. A total of 100 data points were selected from the stable grinding force zone in each direction to evaluate the mean and obtain the corresponding average force. The grinding temperature was determined using a thermocouple. During the data processing, eliminating larger data was necessary to reduce accidental and random errors.

2.4 Experimental results

2.4.1 Specific grinding force

Grinding force is one of the most important grinding parameters during the grinding process. It is closely related to the service life of the grinding wheel, processing quality of the workpieces, and is often used to characterize the lubricating

Table 2 Chemical composition of Ti–6Al–4V

Components	Substrate	Alloy elements (wt%)		Others (wt%)					
Ti–6Al–4V	Ti	Al	V	Fe	Si	C	N	H	O
		5.5–6.8	3.5–4.5	0.3	0.1	0.1	0.05	0.015	0.01

Table 3 Performance parameters of Ti–6Al–4V

Thermal conductivity (W/m·°C)	Specific heat (J/kg·K)	Density (g/cm^3)	Elasticity modulus (GPa)	Poisson ratio	Yield strength (MPa)	Tensile strength (MPa)
7.955	526.3	4.42	114	0.342	880	950

effect on the grinding wheel/workpiece interface [35]. Smaller grinding force indicates smaller energy consumption to eliminate the same volume of materials and better lubricating effect and grinding performance. Grinding force is mainly characterized by tangential and normal grinding forces. Expressions of the specific tangential and specific normal friction forces are as follows:

$$F_t' = \frac{F_t}{b} \quad (1)$$

$$F_n' = \frac{F_n}{b} \quad (2)$$

where F'_t is the specific tangential grinding force (N/mm), F'_n is the specific normal grinding force (N/mm), F_n is normal grinding force (N), F_t is tangential grinding force (N), and b is the width of the grinding wheel in contact with the workpiece. In the experiment, b is the width of the grinding wheel (20 mm). The grinding experiment of 10 strokes was recorded in each cooling condition. A total of 100 grinding data points in the grinding force stable region of each stroke were recorded, and the average value of data points was chosen as the grinding force value of the experiment.

Figure 2 shows the specific grinding force under three different cooling conditions. The error bar represents the standard deviation of grinding force. As shown in Fig. 2, CNMQL has the smallest specific tangential and specific normal grinding forces, which are 2.17 and 2.66 N/mm, respectively. However, the specific tangential and normal grinding forces under NMQL and CA increase to different extents. The specific tangential and normal grinding forces under NMQL are 2.43 and 3.06 N/mm, which are 12.3 and 15.0% higher than those of CNMQL, respectively. CA gains the highest specific tangential grinding force of 3.66 N/mm and specific normal grinding force of 4.36 N/mm, which are 69.1 and 63.9% higher than those of CNMQL, respectively.

Given the shortage of lubricating medium, CA generates substantial grinding force, indicating its higher energy consumption to eliminate the same volume of materials than other cooling conditions. NMQL has excellent lubricating performance in the grinding zone due to the excellent lubricating performance of the nanofluids in the grinding zone; thus, NMQL has smaller grinding force than CA. CNMQL combines the advantages of the two abovementioned cooling conditions and reaches the best lubricating performance. It reduces the grinding force significantly and increases the processing quality of the workpieces.

2.4.2 Grinding temperature

Excessive temperature is one of the main factors that influence and restrict quality of processing parts and service of the grinding wheel. Therefore, the process of cooling the grinding zone effectively and lowering the temperature in the grinding zone are important topics in the grinding process. The grinding experiment of 10 strokes was recorded in each cooling condition. A total of 50 grinding temperature data points at the temperature peak region of each stroke were recorded, and the average value of the data points was chosen as the experimental grinding zone temperature.

Figure 3 shows the measuring curve of the temperature in the grinding zone under three different cooling conditions. Figure 4 shows the grinding temperature under different cooling conditions. As shown in Fig. 4, NMQL achieves the highest temperature, which is 214.1 °C, reflecting the poor cooling performance of NMQL. Considering the excellent cooling and heat exchange performances of cryogenic air, the grinding temperature under CA is 197.5 °C, which is about 17 °C lower than of NMQL. CNMQL integrates the advantages of NMQL and CA, thereby achieving satisfying cooling and lubricating effects. CNMQL achieves the lowest temperature of 155.9 °C, which is about 42 °C lower than that of CA, with a drop of 21%. Compared with NMQL, the temperature of CNMQL was decreased by about 60 °C with a drop of 28%.

Table 4 Physical properties of the Al_2O_3 nanoparticles

Grain size (nm)	Crystal structure	Melting point (°C)	Bulk density (g/cm^3)	Thermal conductivity (W/m·K)	Color	Mohs' hardness
50	Hexagonal close packing	2050	0.33	36	White	8.8–9.0

Table 5 Experimental grinding process parameters

Grinding parameters	Value
Grinding pattern	Surface grinding
Cooling conditions	CA, NMQL, and CNMQL
Peripheral speed of grinding wheel V_s (m/s)	24
MQL flow rate (ml/h)	50
Feed speed V_w (mm/min)	4000
Cutting depth a_p (μm)	10
Total gas flow rate (m^3/h)	25
Nozzle distance (mm)	12
Nozzle angle α (°)	15
Gas pressure P (MPa)	0.7

3 Mathematical model of grinding temperature field

3.1 Heat transfer model

Interaction between grinding particles and workpiece will generate abundant heat in the grinding zone during the grinding process. With continuous feeding of the workpiece, heat source moves forward continuously. Heat diffuses around by centering at the heat source, and heat is at the equilibrium on the axial direction of the grinding wheel. No heat exchange on the axial direction is suggested. Therefore, analysis on the grinding temperature field can be simplified into the two-dimensional heat transfer model (Fig. 5).

According to the first law of thermodynamics and Fourier heat transfer law, the two-dimensional transient temperature field without internal heat source satisfies the following differential equation of heat equilibrium [36]:

$$\left(\frac{\partial^2 T}{\partial x^2}+\frac{\partial^2 T}{\partial z^2}\right)=\frac{1}{\alpha}\frac{\partial T}{\partial t} \tag{3}$$

where α is the thermal diffusion coefficient of the materials (m^2/s), $\alpha = \lambda/(\rho_w \cdot c_w)$, T is the transient temperature of the workpiece (°C), t is the time (s), and ρ_w and c_w are the density (kg/m^3) and specific heat capacity (J/[kg·K]), respectively.

The grinding process is a random cutting process of numerous abrasive particles to the workpiece material. On the grinding direction, the debris thickness is the largest in the very front of the grinding area, decreases gradually, and decreases to zero at the tail of the grinding zone. Therefore, heat flux on the grinding interface between the grinding wheel and workpiece is approximately in triangular distribution. Thus, the triangle moving heat source model was used in this study.

Table 6 Temperature and air flow at nozzle outlet under three cooling conditions

Cooling conditions	Air temperature at the nozzle outlet (°C)	Air flow (m^3/h)
CA	− 5	10
NMQL	25	25
CNMQL	− 5	10

3.2 Energy ratio coefficient

In the surface grinding, the heat source model can be approximately regarded as a process caused by a heat source of infinite width and finite length on the semi-infinite heat conductor. The total heat flux q_{total} in the grinding zone caused by the energy input from the grinding wheel can be calculated using the following equation [35]:

$$q_{total}=\frac{Q}{S}=\frac{F_t \cdot v_s}{l_c \cdot b} \tag{4}$$

where q_{total} is the total heat flux density (J/[m^2·K·s]), Q is the grinding power (J/s), S is contact area between the grinding wheel and workpiece (mm^2), v_s is the linear velocity of the grinding wheel (m/s), l_c is the contact arc length between the workpiece and grinding wheel (mm), and b is the grinding width (mm).

The contact arc length in the grinding zone can be calculated using the following equation:

$$l_c=\sqrt{d_s a_p} \tag{5}$$

where d_s and a_p are grinding wheel diameter (mm) and grinding depth (μm), respectively. The numerical values of the grinding wheel diameter and grinding depth are very small, and the grinding wheel length is generally a several micrometers. Thus, moving direction of the heat source can be viewed approximately parallel to the workpiece. In the grinding process, the total heat flows to workpiece substrate, abrasive particles, grinding debris, and grinding liquid. R is the energy ratio coefficient that is transmitted into the workpiece. R is determined by type of grinding wheel, workpiece material properties, and working conditions. R influences the temperature field in the grinding zone significantly. The calculation formula of the heat flux density, which flows into the workpiece, can be calculated using the following equation:

$$q_w=\frac{q_w}{q_{total}}=\frac{v_s F_t}{b l_c}\cdot R=\frac{v_s F_t}{b\sqrt{d_s a_p}}\cdot R \tag{6}$$

(6)where q_w is the heat flux density transmitted into the workpiece (J/[m^2·K·s]), and q_{total} is total heat flux density (J/[m^2·K·s]).

Energy ratio coefficient R can be calculated using the following equation [37]:

$$\mathrm{R}=\frac{k_w {v_w}^{1/2}}{q_{total}\beta {a_w}^{1/2}{a_p}^{1/4}{d_s}^{1/4}}\theta_{\max} \tag{7}$$

Table 7 Dressing parameters of the grinding wheel

Dresser type	Fixed PCD dresser of the K–P36 grinder
Single stroke trimming amount (mm)	0.01
Transverse feed rate (mm/rev)	0.5
Number of stroke	20

where k is the thermal conductivity coefficient of the workpiece material (W/[m^2·K]), β is a constant determined by the shape of the hat source and is generally 1.06, α_w is the thermal diffusion coefficient of the materials (m^2/s), and θ_{max} is the peak temperature rise (°C).

3.3 Heat transfer coefficient model

Many studies have been conducted on the boiling heat transfer theory [38]. According to the classical thermodynamics theory, temperature in the grinding zone may be higher than the boiling point of the grinding medium after being sprayed onto the high-temperature grinding zone. This temperature difference is depicted as ΔT. When ΔT is higher than the minimum degree of superheat ΔT_s, the grinding zone is in the boiling heat transfer process. The boiling heat transfer is divided into four stages, namely, natural convection, nucleate boiling, transition boiling, and film boiling heat transfer [39, 40]. Different ΔT corresponds to different stages. According to boiling heat transfer mechanism [41], which is the minimum degree of superheat to produce bubbles and the formula of film boiling heat transfer [42], the heat transfer state of the cooling medium in the grinding zone can be determined using the following equations:

$$\Delta T_s = \frac{T_s^2}{B}\lg\left(1+\frac{2\sigma}{rp_s}\right)\left[1+\frac{T_s}{B}\lg\left(1+\frac{2\sigma}{rp_s}\right)\right] \tag{8}$$

$$\Delta T_{\min} = 0.127\frac{\rho_g'\varsigma}{K_g'}\left[\frac{g\left(\rho_g-\rho_l\right)}{\rho_l+\rho_g}\right]^{2/3}\left[\frac{\sigma}{g\left(\rho_g-\rho_l\right)}\right]^{1/2}\left[\frac{\mu_l}{g\left(\rho_g-\rho_l\right)}\right]^{1/3} \tag{9}$$

where ΔT_s is the minimum degree of superheat to produce bubbles (°C), σ is the surface tension (N/m), T_s is the boiling point of the liquid (°C), r is the radius of the concave meniscus formed in the capillary (mm), B is the constant, $p_s = 0.1$ Mpa, $B = 2156$, p_l is density of liquid (kg/m^3), p_g is the air density (kg/m^3), μ_l is the dynamic viscosity of liquids (cP), $\Delta T_{\min}$ is the minimum degree of film boiling heat transfer (°C), p'_g is the gas film density (kg/m^3), K'_g is the air film heat transfer coefficient (kJ/[m·K·s]), and ζ is the latent heat (kJ/kg).

The composition and boiling point of the synthesis lipid, which is used in the experiment, are listed in Table 8. Aromatic hydrocarbon has the largest proportion and lowest boiling point; therefore, the boiling point of the nanofluid is approximately 105 °C.

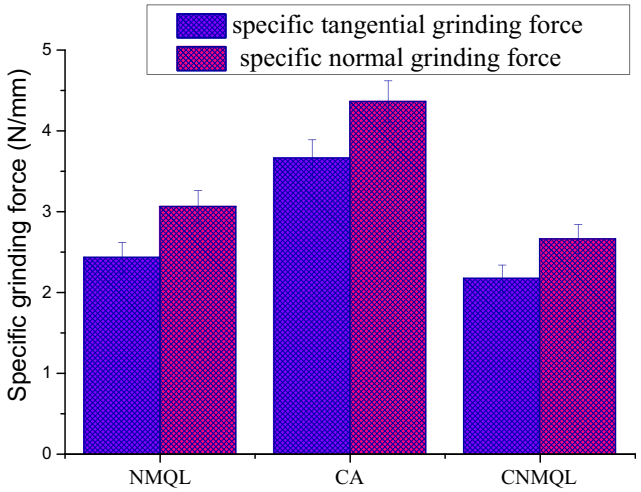

Fig. 2 Specific grinding force under different cooling conditions

Comparing the grinding temperature in three different cooling conditions, we found that CA and NMQL are in the transition boiling heat transfer state, while CNMQL is in the nucleate boiling heat transfer state. Using Eqs. (8) and (9), $\Delta T_s = 2.1$ °C and $\Delta T_{\min} = 122$ °C can be calculated.

When $\Delta T < \Delta T_s$, the forced convection heat transfer by air and natural convection heat transfer by liquid cooling medium are dominant heat transfer modes in the heat transfer state in the grinding zone. Generally, the temperature difference between the nucleate boiling heat transfer state and ΔT_s ranges between 20 and 50 °C [43]. When $\Delta T_s < \Delta T < \Delta T_s + 50$ °C, the interface between the cooling medium and workpiece surface is in the nucleate boiling heat transfer state. When $\Delta T_s + 50$ °C $< \Delta T < \Delta T_{\min}$, the interface between the cooling medium and workpiece surface is in the transition boiling heat transfer state. When $\Delta T_s \geq \Delta T_{\min}$, the interface between the cooling medium and workpiece surface comes into the film boiling heat transfer state. The boiling heat transfer state and heat transfer coefficient corresponding to the temperature in the grinding zone are shown in Fig. 6. The critical point is the critical heat flux density point.

No liquid cooling medium was observed under CA; thus, no boiling heat transfer state is present. The heat transfer process that was observed is only the forced convection heat transfer between cryogenic air and the workpiece surface. The convection heat transfer coefficient h_a between air and wall can be calculated using the following equation [44]:

$$\begin{cases} h_a = \lambda_a N\mu/l \\ Nu = 0.906\mathrm{Re}^{1/2}\mathrm{Pr}^{1/3} \\ \mathrm{Re} = v' a p_a l/\mu_a \\ \mathrm{Pr} = \mu_a c_a/\lambda_a \end{cases} \tag{10}$$

where λ_a is the thermal conductivity of air (W/[m^2·K]), Nu is Nusselt number, l is the heat transfer width in the grinding

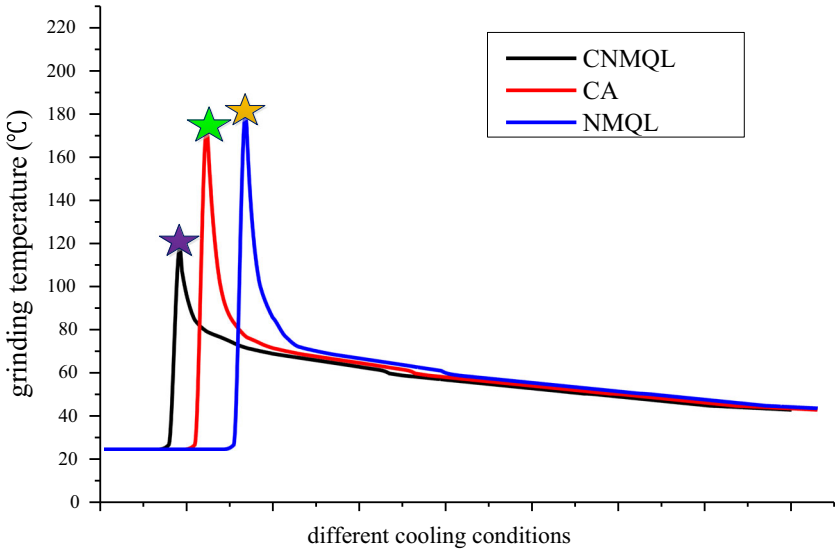

Fig. 3 Measuring the curve of temperature under different cooling conditions

zone (mm), *Re* is Reynolds number, *Pr* is Prandtl number, v'_a is the gas velocity, ρ_a is the gas density (kg/m^3), μ_a is the gas dynamic viscosity (cP), and c_a is the air pressure specific heat capacity (J/[kg·K]).

The nucleate boiling and transition boiling heat transfer states in the boiling heat transfer process both present a linear variation trend. The heat transfer coefficient under different working conditions can be calculated using the linear interpolation method. In the NMQL grinding condition, the temperature of the grinding zone is 214.1 °C; at this moment, the single nanofluid droplet which is sprayed to the workpiece is in the transition boiling heat transfer state. The heat transfer coefficient under NMQL is solved by dividing it into four stages:

(1) Natural convection heat transfer state

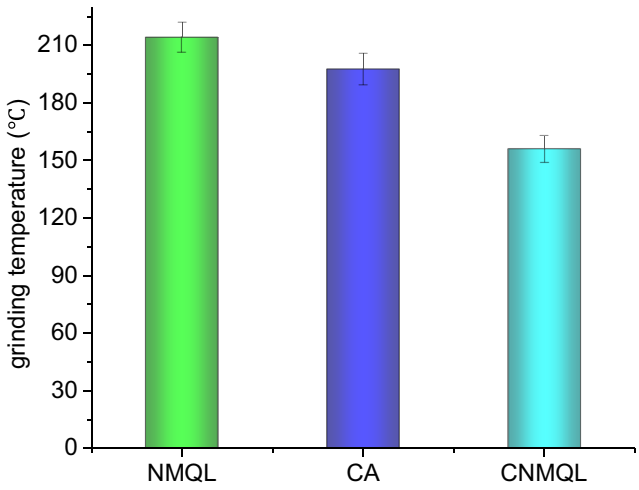

Fig. 4 Grinding temperature under different cooling conditions

When the workpiece surface temperature T is less than 107.1 °C, no boiling heat transfer is generated on the heat transfer surface [37]. Instead, the forced convection heat transfer is mainly controlled by the ambient temperature air and nanofluids, where the convective heat transfer of nanofluids is dominant. Nanofluids are sprayed onto the grinding zone through a MQL device. The nanofluids ejected in unit time are discretized into N_l liquid droplets with a volume of V_l that can be calculated as follows [45]:

$$\begin{cases} V_1 = \dfrac{{r_{surf}}^3}{\dfrac{\pi}{2}\dfrac{1}{tg\theta_n}\left(\dfrac{1}{\cos\theta_n}-1\right)\left[1+\dfrac{1}{3}\dfrac{1}{tg^2\theta_n}\left(\dfrac{1}{\cos\theta_n}-1\right)^2\right]} \\ V_1 = \dfrac{\pi {d_0}^3}{6} \\ N_l = \dfrac{Q'\cdot t}{V_l} \\ t = \dfrac{a}{v_w} \end{cases} \tag{11}$$

where Q' is supply amount of nanofluids per unit grinding time (μm^3/s), r_{surf} is the pavement radius of a single droplet (μm), N_l is the quantity of droplets, t is the total grinding time (s), a is the length of the workpiece (μm), v_w is the feed rate of the workpiece (μm/s), V_l is the volume of a single droplet (μm^3), d_0 is the spherical diameter of a single droplet (μm), and θ is the contact angle (°).

According to Yang's findings on the no-boiling heat transfer coefficient [13], the following formula can be expressed as follows:

$$h_{n1} = \frac{N_l c_l \rho_l V_l}{\pi {r_{surf}}^2 \cdot t} + h'_a \tag{12}$$

Table 8 Composition and boiling point of the synthesis lipid

Components	Aromatic hydrocarbon	Pentaerythritol adipate	Pentaerythritol ester	Trimethyl phosphate
Content (%)	60	20	10	10
Boiling point (°C)	105	109	380.4	265

where N_l is the quantity of droplets, c_l is the specific heat capacity of droplets (J/[kg·K]), ρ_l is the density of the nanofluid (kg/m^3), V_l is the volume of a single droplet (μm), r_{surf} is the pavement radius of a single liquid drop (μm), T_s is the saturation temperature (K), and h'_a is the convective heat transfer coefficient of room temperature air (W/[m^2·K]). Moreover, h'_a can be calculated according to the equation of convective heat transfer coefficient between gas and wall. The following parameters are known: $N_l = 7800$,$c_l = 1870$ J/(kg·K), $\rho_l = 665$ kg/m^3, $V_l = 2.14 \times 10^{-12}$ m^3, $r_{surf} = 1.2 \times 10^{-4}$ m, $T_s = 105$ °C, and $h'_a = 278$ W/m^2·K.

(2) Nucleate and transition boiling heat transfer states

h reaches the maximum h_{n2} at the tail point of the nucleate boiling heat transfer state and the initial point of the transition boiling heat transfer state, which is called the critical heat flux density point ($T_{n2} = 157.1$ °C). h reaches the minimum at the tail stage of the transition boiling heat transfer, which is called the starting point ($T_{n3} = 227$ °C) of the film boiling heat transfer state. The critical heat flux point heat transfer coefficient h_{n2} can be calculated as follows [46]:

$$h_{n2} = \frac{\left[h_{fa} + c_l(T_s - T_l)\right] Q' \rho_l}{\pi r_{surf}{}^2 (T_{n2} - T_l)} + h'_a \tag{13}$$

where q'_a is the convection heat transfer of air at room temperature (J/[m^2·K·s]), N_l is the amount of evaporated liquid drops, c_l is the specific heat capacity of droplets (J/[kg·K]), h_{fa} is the latent heat of vaporization (kJ/kg), T_s is the saturated temperature (K), T_{n2} is the starting point temperature of the transition boiling heat transfer (K), and T_l is the temperature of nanofluids (K).

(3) Transition and film boiling heat transfer states

The heat transfer coefficient h_{n3} at the initial point of film boiling state can be expressed as [48]:

$$\begin{cases} h_{n3} = \dfrac{N_l Q' \rho_l \left[h_{fa} + c_l(T_s - T_l)\right] \cdot \left[0.027 e^{\frac{0.08\sqrt{\ln(We/35+1)}}{B^{1.5}}} + 0.21 k_d B e^{\frac{-90}{We+1}}\right]}{b \cdot l_c \cdot (T_{n3} - T_l)} + h'_a \\ We = \dfrac{\rho_l d_0 v_n^2}{\sigma} \\ v_n = \sqrt{\dfrac{p_a - p_0}{\rho_l} + \dfrac{16 Q'^2}{\pi^2 d_0^2}} \cdot \dfrac{\cos\theta}{1+\varepsilon} \\ B = \dfrac{c_v (T_{ne} - T_s)}{h_{fa}} \\ l_c = \sqrt{a_p \cdot d_s} \\ k_d = \dfrac{\lambda_v}{c_v \mu_v} \end{cases} \tag{14}$$

where p_a is the internal pressure in the nozzle (Pa), p_o is the barometric pressure (Pa), v_l is the effluent velocity of droplets along the nozzle direction (m/s), v_n is the vertical velocity when droplets affect the heat convection surface (m/s), b is the width of the grinding zone (mm), l_c is the contact arc length (mm), λ_v is the thermal conductivity of steam (W/[m·K]), μ_v is the steam viscosity (cP), c_v is the thermal capacity of mass (J/[kg·K]), θ is the included angle between the droplets' efflux and horizontal directions (°), and σ is the surface tension (N/m).

Coefficients that are calculated by formulas/equations mentioned above are shown in Table 6. The temperature at the starting point of nucleate boiling (T_{n1}) is 107.1 °C ($h_{n1} = 3.8 \times 105$ W/m^2·K). The temperature at the end point of nucleate boiling, which is called the initial point of transition boiling, T_{n2} is 157.1 °C ($h_{n2} = 8.2 \times 105$ W/m^2·K). The temperature at the tail point of transition boiling, which is called the initial point of film boiling, (T_{n3}) is 227 °C ($h_{n3} = 2.92 \times 105$ W/m^2·K).

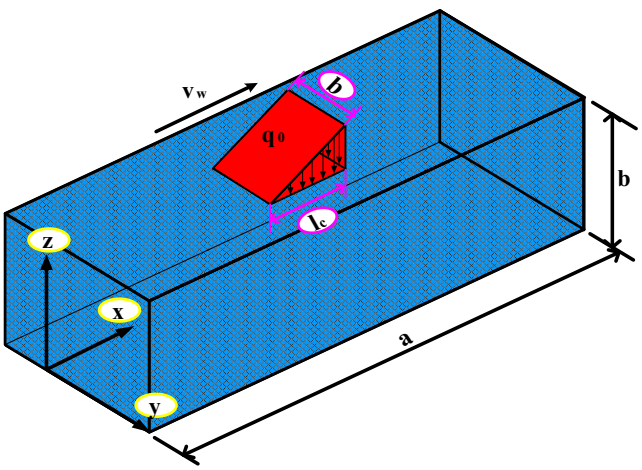

Fig. 5 Heat transfer model

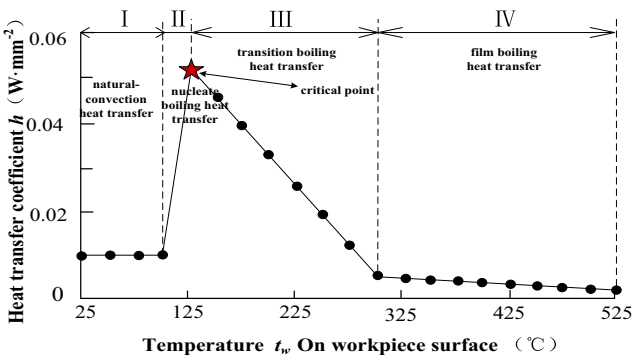

Fig. 6 Schematic diagram of the boiling heat transfer stages

Through interpolation calculation, when the workpiece surface temperature T is 214.1 °C, the coefficient of heat transfer can be calculated as follows: $h_n = 3.74 \times 105$ W/m^2·K. The given parameters are shown in Table 9, and the schematic diagram of the heat transfer coefficients is shown in Fig. 7.

Similarly, h at different turning points in different stages of heat convection state under CNMQL can be calculated using the same method. Then, the actual h of the stage can be calculated using the interpolation method. Using the calculation, the heat transfer coefficient under three different conditions is obtained, as shown in Table 10.

4 Model simulation

4.1 Establishment of the difference equation

The workpiece is simplified into a two-dimensional rectangle plane and is discretized into a plane uniform gridding structure by finite difference method, namely, $\Delta x = \Delta z = \Delta l$. As shown in Fig. 8, intersection points of the gridding lines are called nodes. The intersection points between the grinding lines and object boundaries are the boundary nodes. The temperature at each node represents the temperature of the grid unit. Use a point inside the workpiece (i, j) as an example. All adjacent the nodes $(i-1, j)$, $(i+1, j)$, $(i, j-1)$, and $(i, j+1)$ have contact with this node (i, j). According to the first law of thermodynamics, heat at this node will result in heat conduction with the surrounding adjacent nodes. Heat transfer ends at the equilibrium of heat transfer, finally reaching the stable temperature.

On the basis of the principle of replacing differential quotient with difference quotient, the finite difference method causes the differential discretization to partial differential equation and boundary conditions of the field domain. The finite difference equation set is established based on the second-order difference quotient. The established equation set is as follows:

$$\begin{cases} \dfrac{\partial^2 T}{\partial x^2}(i,j) = \dfrac{T(i+1,j) - 2T(i,j) + T(i-1,j)}{\Delta x^2} + \mathrm{O}(\Delta x^2) \\ \dfrac{\partial^2 T}{\partial z^2}(i,j) = \dfrac{T(i,j+1) - 2T(i,j) + T(i,j-1)}{\Delta z^2} + \mathrm{O}(\Delta z^2) \\ \dfrac{\partial T}{\partial t}(i,j) = \dfrac{T_{t+\Delta t}(i,j) - T_t(i,j)}{\Delta t} + \mathrm{O}(\Delta t) \end{cases} \tag{15}$$

Table 9 Given parameters

Parameters	Value
d_0	160 μm
N_l	7800
h'_a	278 W/m^2·K
v_n	10.8 m/s

where $T(i, j)$ is the temperature at point (i, j), while $T_t(i, j)$ and $T_{t+\Delta t}(i, j)$ represent temperatures of point (i, j) at times t and $t + \Delta t$, respectively. Δt is the time increment, and O represents the infinitesimal quantity. This difference equation set is brought by the heat transduction equation under the two-dimensional space state, thus deducing the difference equation at different nodes in the grind, as follows:

$$T_{t+\Delta t}(i,j) = \frac{\alpha \Delta t[T(i+1,j) + T(i-1,j) + T(i,j+1) + T(i,j-1)]}{\Delta l^2} + \frac{\Delta l^2 - 4\alpha \Delta t}{\Delta l^2} T(i,j) \tag{16}$$

4.2 Boundary conditions of temperature field

With respect to the boundary condition analysis of the grinding zone, we used the coordinate point $(i, 1)$ on the surface of workpiece as an example. As shown in Fig. 9, the heat input on the grinding wheel–workpiece interface during the grinding process, heat transfer between different nodes, temperature rise of node itself, and convection heat transfer among the workpiece grinding surface, cooling liquid, and surrounding air obey to the law of conservation of energy, which can be expressed as follows:

$$q_{(i-1,1)\to(i,1)} + q_{(i+1,1)\to(i,1)} + q_{(i,2)\to(i,1)} + qA = \rho_w C_w V_0 \frac{\partial T}{\partial t} + GA\left[T_{i,1} - T_a\right] \tag{17}$$

where $T(i,1)$ is the temperature at node $(i,1)$, T_a is the temperature of the cooling liquid or surrounding air, V_0 is the unit grid volume, $V_0 = \Delta x \cdot \Delta Z \cdot 1 = \Delta l^2$, G is the comprehensive coefficient of heat transfer, $G = [1/h] + \Delta Z/(2\ k)]^{-1}$, A is the surface area per unit grid, and $A = \Delta x \cdot 1 = \Delta Z \cdot 1 = \Delta l$. The heat transfer between the nodes $(i-1,1)$ and $(i,1)$ can be expressed as follows:

$$q_{(i-1,1)\to(i,1)} = k(\Delta z \cdot 1)\left(\frac{T_{i-1,1} - T_{i,1}}{\Delta x}\right) = k\left(T_{i-1,1} - T_{i,1}\right) \tag{18}$$

Similarly, the heat transfer between nodes $(i+1,1)$ and $(i,1)$, $(i,2)$, and $(i,1)$ can be expressed as follows:

$$q_{(i+1,1)\to(i,1)} = k\left(T_{i+1,1} - T_{i,1}\right) \tag{19}$$

$$q_{(i,2)\to(i,1)} = k\left(T_{i,2} - T_{i,1}\right) \tag{20}$$

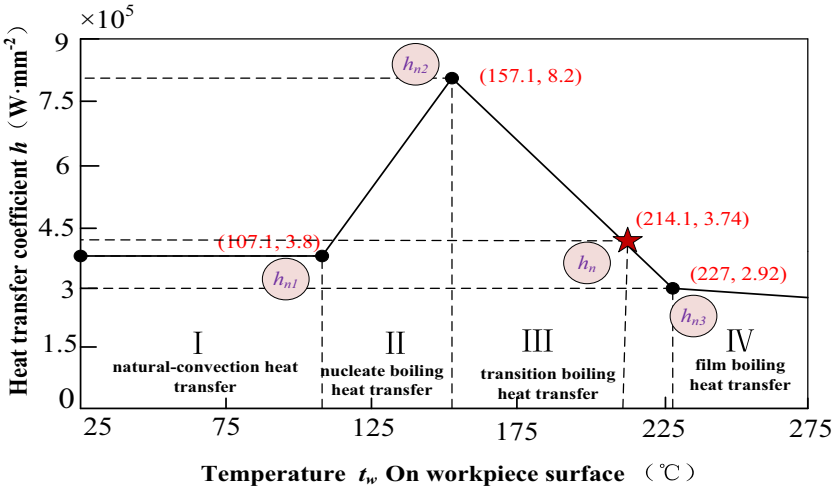

Fig. 7 Schematic diagram of the boiling heat transfer under NMQL condition

Merging the three previous formulas into Eq. (17), the temperature at node $(i,1)$ after Δt can be calculated as follows:

$$T_{t+\Delta t}(i,1) = \frac{\Delta t}{\rho_w C_w \Delta l^2}\{k\cdot[T(i-1,1)+T(i+1,1)+T(i,2)-3T(i,1)]+[q-G(T_t-T_a)]\cdot\Delta l\}+T(i,1) \quad (21)$$

In the same way, the temperature rise on the other boundary positions can be analyzed and solved by the heat balance equation. This experiment is accomplished under room temperature. Therefore, the initial temperature $T_{t=0}$ is 20 °C.

4.3 Simulation results

A simulation analysis on the temperature field on the workpiece surface under three cooling conditions was carried out using Matlab simulation platform. The numerical simulation diagrams of the grinding temperature distribution of the heat source with time from cutting in to cutting out in the grinding zone under CNMQL are shown in Fig. 10. The results of grinding temperature changing with time at one point of the workpiece under different cooling conditions are shown in Fig. 11. As shown in Figs. 10 and 11, the grinding temperature in the grinding wheel/workpiece contact zone is the highest (red zone). However, the temperature will decrease gradually after the heat source passes through. Temperature mainly concentrates in the heat source point and in the region where the heat source passes through. Unprocessed surface has no significant temperature difference. Given the low heat conductivity coefficient of the Ti alloy, the temperature at the grinding point is close to environmental temperature before the grinding wheel reaches it. The temperature on the workpiece surface increases sharply when the grinding wheel reaches the grinding point. However, the temperature at this point declines gradually after the grinding wheel leaves this point until it reaches the temperature close to the environment. Theoretical result conforms to the grinding temperature changing law in the actual grinding process.

Table 10 Heat transfer coefficient under different cooling conditions

Cooling conditions	T (°C)	h (W/m^2·K)
NMQL	214.1	3.74×10^5
CA	197.5	221
CNMQL	155.9	4.38×10^5

4.4 Comparison between the simulation and experimental results

Comparison between experimental and theoretical temperature of workpiece surface under CNMQL is shown in Fig. 12. The theoretical result agrees with the experimental result. The theoretical result of the highest temperature on the workpiece surface is compared with experimental value. The temperature difference between the experimental and theoretical values under CNMQL is only 5.1% (7.9 °C), which is in the reasonable range. Meanwhile, the theoretical temperature on the workpiece surface is higher than the experimental value. The reason may be as follows [39]: during the simulation calculation, the model hypothesizes that heat transferred into the workpiece would not diffuse and enter into the external environment; in actual situations, the heat entering into the workpiece will continue to transfer inside the workpiece, and a

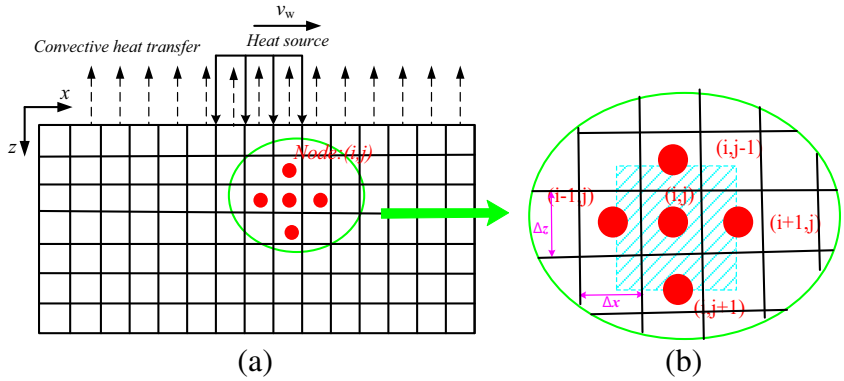

Fig. 8 Plane uniform gridding structure

portion will transfer into lateral side of the surfaces of the workpiece material; simultaneously, a portion of heat on the workpiece surface will be carried away by the grinding liquid and surrounding air, thereby decreasing the actual heat entering into the workpiece material; thus, the actual temperature will be lower than the theoretical value. In general, theoretical result agrees highly with the experimental temperature, indicating that the model is reliable to some extent.

5 Discussions

5.1 Evaluations of cooling performances under different cooling conditions

On the basis of the comparison of grinding temperature in the grinding zone under three cooling conditions, we can conclude that CNMQL has the best cooling performance, followed by CA and NMQL.

Under the NMQL grinding condition, although the dosage of minimal quantity of lubricant is only 1/1000 of that in the traditional pouring lubrication, high pressure air carrying nanofluid grinding liquid can break the air barrier layer and enter into the grinding zone effectively, forming a lubricating oil film [3, 4]. This film can offer good lubricating effect during the grinding process, manifested by reduction in the grinding force and heat to some extent. Al_2O_3 is a tightly packed crystal material of six parties. It has high hardness, heat resistance, and wear resistance. In the lattice of α–Al_2O_3, the oxygen ions are tightly packed by six parties, and Al^{3+} is symmetrically distributed in the eight surface coordination centers that are surrounded by oxygen ions. The lattice has high energy; thus, the melting and boiling points of Al_2O_3 are very high. The physical properties of the Al_2O_3 nanoparticles are shown in Table 4 above. The melting point of Al_2O_3 can reach 2050 °C and has good heat resistance. The addition of Al_2O_3 nanoparticles improves the high-temperature stability of the lubricating film and enhances the high-temperature tribological performance of the lubricating film. Meanwhile, the Mohs' hardness of Al_2O_3 can reach 8.8 to 9.0, and the Al_2O_3 nanoparticles with high hardness have excellent wear resistance. In the grinding process, Al_2O_3 nanoparticles can play a supporting role in the friction surface. The properties of Al_2O_3 nanoparticles can also significantly improve the cooling and lubricating performance of the nanofluid lubricating oil. At the same time, the lubricating oil film formed by the nanofluids in the grinding zone prevents heat from being introduced into the workpiece to some extent. The cooling mechanism is based on the forced convection of the room temperature air and boiling heat transfer of the minimal quantity lubricating oil under high temperature by taking away heat to reduce the temperature of the grinding zone. The cooling performance is insufficient, thereby achieving the highest grinding temperature.

CA achieves lower grinding temperature than that of NMQL. Without the lubricating medium, CA fails to form satisfying lubrication performance in the grinding contact zone, which needs substantial grinding force consumption to eliminate the workpiece material, as well as high heat consumption. For the cooling mechanism, the CA cooling performance under the CA and room temperature air under NMQL in the grinding zone all belong to the forced convection heat transfer. However, the temperature of high-pressure air, which causes the forced convection, is different. CA uses the cryogenic high-pressure air as the carrying medium, which enlarges the temperature difference between the medium and grinding contact surface and strengthens the convection heat transfer effect. Although CA lacks a lubricating medium, it consumes tremendous heat during the material removal; the excellent cooling and heat exchange capacity of CA offsets

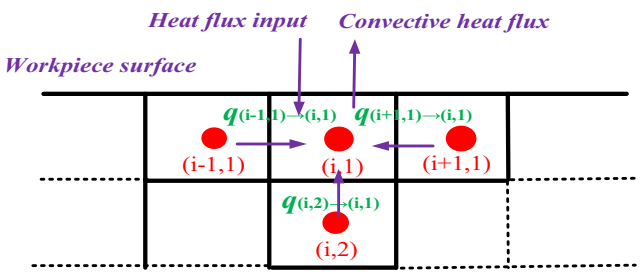

Fig. 9 Heat transfer state at node (*i*,1)

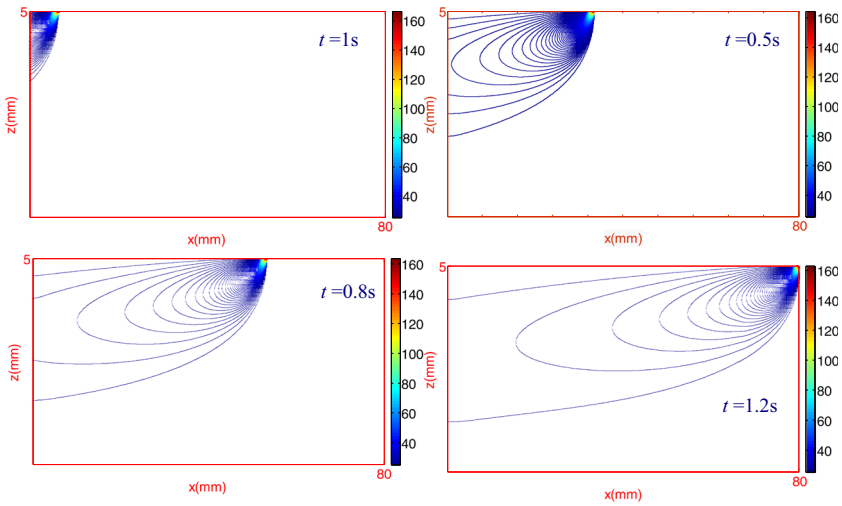

Fig. 10 Simulation grinding phase diagram

this disadvantage. Therefore, CA achieves better cooling effect than NMQL.

CNMQL integrates the advantages of NMQL and CA to achieve the best cooling lubricating effect; thus, the lowest grinding temperature is obtained. The cooling effect of CNMQL is superior to that of NMQL and CA in terms of the cooling effect for the following reasons. Firstly, the lubricating effect of the grinding liquid under CNMQL is better than that under NMQL. Thus, the grinding liquid consumes fewer heat during the grinding process under CNMQL than under NMQL. Second, the nanofluid properties change with the change in the temperature in the grinding zone. The lower grinding zone temperature enables the formation of lubricating film with better lubricity in the grinding contact area, which reduces energy consumption during the grinding process and achieves the best lubricating effect. With the decrease in temperature, the viscosity of liquid increases. The temperature in the grinding area under CNMQL condition is reduced by about 60 °C compared with that of NMQL, and higher viscosity is achieved. With higher viscosity, the lubricating oil in the grinding wheel/workpiece interface exhibits excellent viscous properties. In addition, the formed lubricating film is relatively thick, and its lubricating performance and time are improved, thereby effectively reducing the energy consumption in grinding. On the other hand, under NMQL condition, the nanofluid viscosity is relatively low due to the high temperature in the grinding area. The viscous properties of the lubricants are inferior to that of the former. The formed lubricating film is relatively thin, and the lubricating effect is relatively no good; thus, the energy consumption is relatively high.

Considering the inadequate heat transfer capacity of NMQL, the lubricating oil film is very easy to be broken under high temperature, which deteriorates the lubricating performance and increases the grinding force and heat input. CA involvement increases the stability of the lubricating oil film and reduces the grinding heat input. On the other hand, its heat transfer effect is better than that of NMQL and CA under the effect of CA. The temperature in the grinding zone is only 155.9 °C under NMQL condition, and it is reduced by about 60 °C compared with NMQL. Under NMQL condition, cryogenic high-pressure air is used as the heat carrying medium, which expands the temperature difference between the heat transfer medium and grinding wheel/workpiece contact zone. Therefore, cryogenic high-pressure air is superior to the room temperature air in terms of the forced convection heat transfer effect. It can carry away more heat from the grinding zone than the room temperature air, and it can also reduce temperature in the grinding zone.

5.2 Boiling heat transfer analysis

In the process of removing heat from the grinding zone, most heat is carried away by boiling heat transfer of the grinding liquid, except for a few amount that is carried away by forced convection of air in the grinding zone. When the grinding temperature reaches a specific value, the grinding liquid will be boiled and vaporized in the grinding zone [47, 48]. Mao et al. [46] studied the heat transfer mechanism on the workpiece surface during the grinding process and established a boiling convection model on the workpiece surface. Boiling heat transfer is a heat transfer method where the cooling

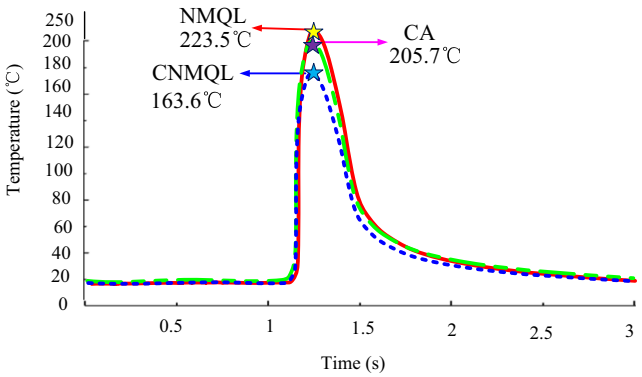

Fig. 11 Theoretical result of the grinding temperature changing with time

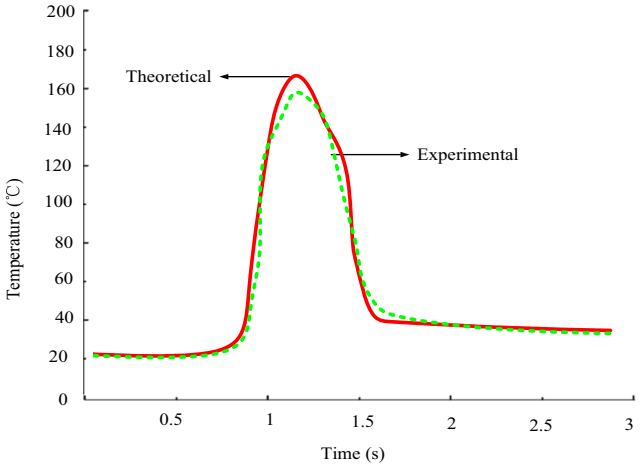

Fig. 12 Comparison of the experimental and theoretical temperatures under CNMQL condition

medium carries away heat by bubble movement and cools the workpieces. Boiling heat transfer in the grinding zone is a violent vaporization process that produces and expands abundant bubbles in the grinding zone and transforms the working medium from liquid state into gas state. It is accompanied by heat transfer through the gas–liquid transformation of the grinding liquid. According to the flow characteristics of the boiling liquid, the boiling heat transfer can be divided into pool and flow boiling. Boiling heat transfer during the grinding process can be viewed as flow boiling heat transfer approximately. Simultaneously, nanofluid cooling liquid undergoes directional migration due to the carrying effect of the cryogenic high-pressure gas, thereby generating boiling heat transfer in the high-temperature grinding zone [49]. Schematic diagram of boiling heat transfer in the grinding zone is shown in Fig. 13. At the beginning of boiling heat transfer in the grinding process, the grinding liquid absorbs the latent heat on the workpiece and grinding debris pipeline pits and surface cracks, which forms the evaporation core [50]. With continuous transfer of heat from the high-temperature surface to the evaporation core, the bubble volume increases continuously until the workpiece surface is left under the effect of floating force and carrying away heat. During the continuous supply of the grinding liquid by the cryogenic high-pressure air, numerous bubbles are formed, grown, and finally vaporized to carry away the grinding heat. This process repeats continuously until the temperature in the grinding zone is finally lowered.

The liquid boiling heat transfer generally can be divided into two stages, namely, vaporization–absorption latent heat and vaporization–evaporation heat transfer. Latent heat refers to the heat that is absorbed or released when the materials transit from one phase to another under fixed temperature; it is also a quantity of state. When the materials absorb (or release) latent heat, they would not cause an increase or decrease in the temperature, and such heat only has potential influences on the temperature changes. Latent energy covers two parts, namely, internal energy difference between two phases (internal latent heat) and power made to overcome the external intensity of pressure at the phase transition (external latent heat). Some absorbed latent heat at liquid boiling are used to overcome the molecular attraction, while rests are used to resist the power of atmospheric pressure during the expansion process. If U_1 and U_2 are used to express the internal energies of phases 1 and 2 of the unit mass, then V_1 and V_2 are used to express their volume of unit mass. The absorbed phase transition latent heat, which is absorbed when the unit mass material transited from phase 1 to phase 2, can be expressed as follows:

$$I = (U_2 - U_1) + (V_2 - V_1) = H_2 - H_1 \tag{22}$$

where h_1 and h_2 are the entropies per unit mass of phases 1 and 2, respectively; $(U_2 - U_1)$ is the internal latent heat absorbed by vaporization–absorption of the liquid; and $p \cdot (V_2 - V_1)$ is the external latent heat absorbed by vaporization–absorption of the liquid. The initial temperature of the cooling liquid (− 5 °C), which is carried by cryogenic air under CNMQL, is lower than that carried by room temperature air (25 °C) under NMQL. In addition, the average initial volume of the vaporization core in the former is smaller; when the volume of the vaporization core increases, more energy is needed; thus, the internal latent heat $(U_2 - U_1)$ during the latent heat adsorption process of the former is higher than that of the latter. At the same time, with the increase in temperature, the liquid molecules will have higher kinetic energy, and the difference between the gas and liquid phases decreases gradually. Thus, the liquid needs less energy from the outside to vaporize. The grinding temperature of the former (155.9 °C) is significantly lower than that of the latter (214.1 °C). Therefore, the heat adsorbed from the grinding zone in the vaporization absorption latent heat process under CNMQL is much higher than that of NMQL condition.

In the vaporization–absorption latent heat process, liquid can only absorb heat from the grinding zone, and temperature remains constant. Then, the liquid enters into the vaporized heat transfer process. Heat transfers from high-temperature surface into the vaporization core continuously. Bubble volume expands, and the temperature increases continuously until leaving the workpiece surface as well as carrying away heat under the effect of buoyancy. So far, the boiling heat transfer process is finished. Given the same specific heat of the cooling liquid, the temperature difference Δt between the evaporation latent heat stage to the evaporation temperature under CNMQL is higher than that of NMQL. The absorbed heat during this process is also much higher than the NMQL. On the basis of the analysis above, the heat that was carried away under CNMQL from the grinding zone into the boiling heat transfer process is much higher than that of NMQL, indicating that CNMQL has better comprehensive heat transfer effect than NMQL.

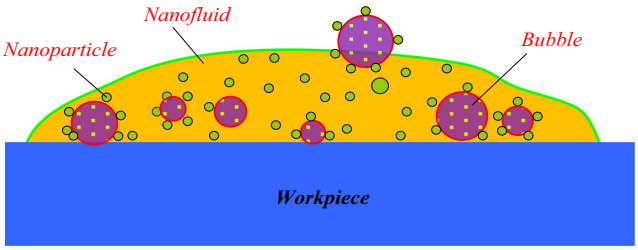

Fig. 13 Boiling heat transfer in the grinding zone

5.3 Influence of surface characteristics of the workpiece and chip on the cooling effect

In the grinding process of the metal materials, the key for grinding liquid to develop the best cooling effect effectively lies in the full pavement to the whole grinding zone, carrying away heat from the grinding zone through the boiling heat transfer. A strong air barrier layer will be formed surrounding the grinding wheel, which is rotating at a high speed; thus, only 5 to 40% of the grinding liquid can reach the grinding zone. On the other hand, the rest of the grinding liquid is prevented from the grinding zone and can only offer local cooling performance of the workpiece, resulting in poor cooling effect in the grinding zone, burn damages of the workpieces, and poor surface quality [12, 13].

The grinding surface is composed of abundant irregular scattered abrasive particles, which plows with different depths. Thus, plastic deformation layer and microcracks will be developed on the workpiece surface during the grinding process. Meanwhile, some grinding debris cannot leave the grinding zone in time. These grinding debris are also easy to adhere onto the workpiece surface again under high temperature to form microbulges. These interface frictional characteristics form the microlevel pipelines with different depths on the grinding wheel and workpiece surface. Microstructures of the workpiece surface under NMQL and CNMQL conditions are shown in Fig. 14. Significant differences have been observed under different conditions. Evident plastic deformation layer and long deep plows on the workpiece surface under NMQL is observed, accompanied with serious adhesion and material sedimentation. As a result, the longitudinal flow of the lubricants along the pipe and the horizontal spreading effect between the pipes are hindered to a certain extent, which affects the overall infiltration effect of the lubricants on the grinding surface, reduces the lubricating effect, and consumes great energy in the process of material removal. When the abrasive particles are embedded in the surface of the workpiece in the grinding process, the furrows are formed due to the poor lubricating effect on the workpiece surface. Under high temperature and pressure, the displacement between the metal crystal occurs, and plastic plow is formed, and metal particles are deposited onto the both sides of the furrows on the workpiece again by adhesion, thereby forming the plastic deformation layer.

Clear and smooth grinding lines, as well as slight plastic deformation and material adhesion, are present on the workpiece surface under CNMQL; however, no plows are detected. A small barrier is present against the flow and pavement of the lubricating liquid along the line. Thus, better lubricating performances are achieved, and less energy is consumed during the grinding process. Simultaneously, when grinding debris are eliminated along the rotating direction of grinding wheel, the microlevel pipelines will be formed on the grinding wheel abrasive debris contact surface due to friction and plowing. During the grinding process, the cryogenic cooling fluids, which are constantly sprayed from the nozzle, will enter into these microlevel pipelines continuously. The grinding liquid flows into the microlevel pipelines and flows forward quickly due to high kinetic energies brought by high-pressure air. This phenomenon forms cooling oil film on the workpiece and grinding debris surface with good spreading effect [3, 4]. The microlevel pipelines on the workpiece surface are shown in Fig. 15.

On the other hand, the geometric shape of the microlevel pipelines on the workpiece and grinding debris surface can significantly increase the spreading and dynamic heat exchange area of the cooling liquid. Workpiece material experiences continuous friction, plowing, and cutting effects of the grinding wheel during the grinding process. Thus, the workpiece material undergoes plastic deformation, accompanied with crystal slippage and dislocation interweaving, stretching, destroying, and fibering of the crystals. The residual stress and hardening phenomena occur in metals, which makes the grinding debris curl up gradually and forms corrugated

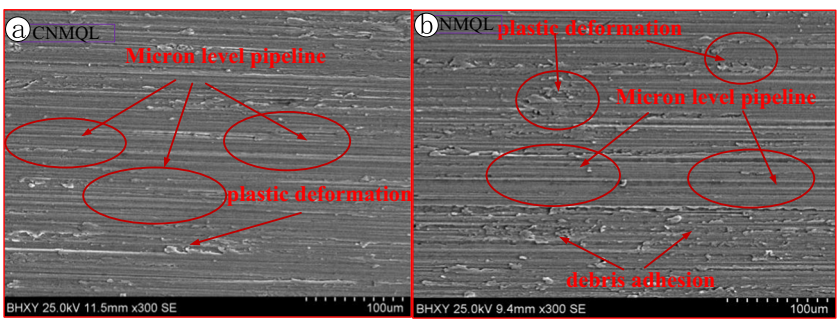

Fig. 14 Workpiece surface microstructures under NMQL and CNMQL conditions

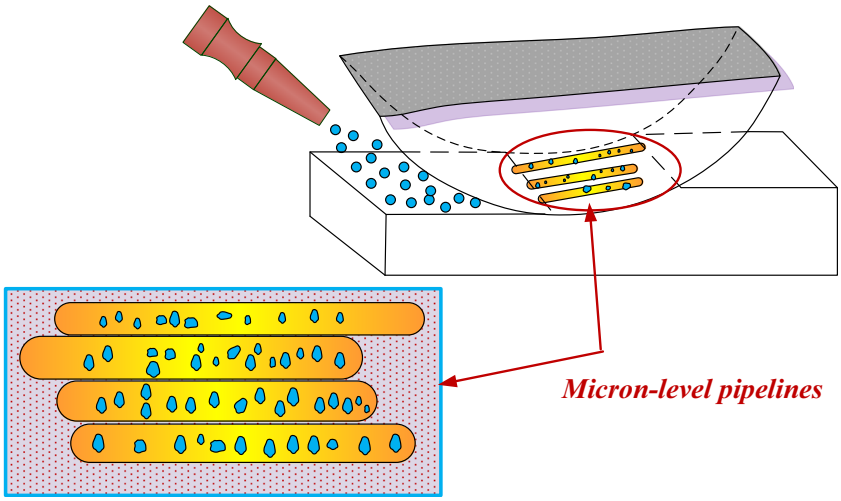

Fig. 15 Microlevel pipelines on the workpiece surface

ditches. The geometric shape of these corrugated ditches increases the surface area of the grinding debris dramatically. The grinding debris microstructures in the bottom surface are shown in Fig. 16. The geometric shape of the workpiece and grinding debris surface expands spreading and dynamic heat transfer area of the cooling liquid. Thus, more cooling liquid can carry away heat from the grinding zone through the boiling heat transfer, thereby achieving the cooling and heat exchanging function.

The total heat transfer amount of the grinding zone is expressed as follows:

$$\phi = qA = Ah\Delta t \tag{23}$$

where q is the heat transfer amount per unit time and area between the solid surface in the grinding zone and heat transfer fluid (J/[m^2·K·s]), A is the heat transfer area in the grinding zone (mm^2), h is the heat transfer coefficient (W/[m^2·K]), and Δt is the temperature difference between the grinding zone and cooling fluid (°C). CA increases Δt between the grinding zone and cooling fluid. Compared with the traditional working conditions, h under CNMQL condition is much higher. The morphological characteristics of the workpiece and grinding debris increase the dynamic heat transfer area A in the grinding zone, which increases the total heat exchange in the grinding zone. Cooling effect is improved significantly compared with the traditional conditions. On the basis of the analysis above, CNMQL achieves the best cooling effect due to the collaborative effect of CA and nanofluid cooling fluid.

6 Conclusion

Theoretical analysis and experimental study on the temperature field during the Ti–6Al–4V grinding process under three cooling conditions (CA, NMQL, and CNMQL) were carried out. The cooling performance under different cooling conditions was analyzed from the grinding mechanism. Thus, the following conclusions are drawn:

(1) On the basis of theory of boiling heat transfer and conduction, a heat transfer coefficient model and a finite difference model under different grinding conditions were established, and the temperature field in the grinding zone under different cooling conditions was simulated. The results showed that CNMQL exhibits the best cooling effect, followed by CA and NMQL.

(2) On the basis of model simulation, the experimental verification of the surface grinding temperature field under cooling conditions of CA, MQL, and CNMQL was carried out by using Ti–6Al–4V as the workpiece material. The results showed that CNMQL has the smallest specific tangential and normal grinding forces (2.17 and 2.66 N/mm) and lowest temperature in the grinding zone

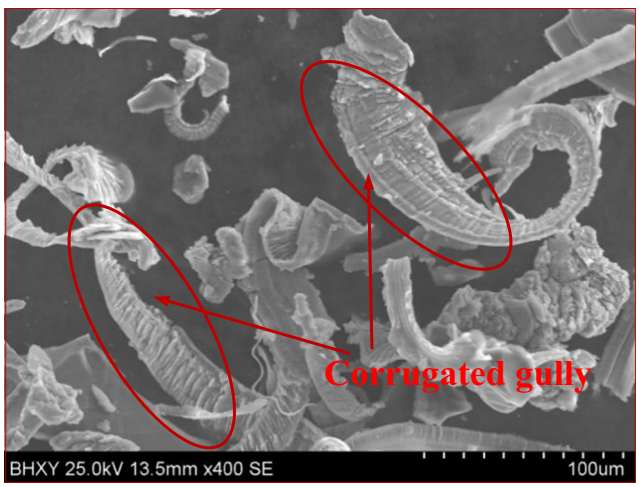

Fig. 16 Grinding debris microstructure in the bottom surface

(155.9 °C), which verified the excellent cooling and heat transfer effects of CNMQL grinding. In addition, the simulation temperature is slightly higher than the experimental temperature. In general, the experimental results are in agreement with the theoretical analysis, which validated the correctness of the theoretical model.

(3) The temperature in the grinding zone under CNMQL condition is reduced by about 60 °C compared with that of NMQL; in addition, higher viscosity is achieved. With higher viscosity, the lubricating oil in the grinding wheel/workpiece interface exhibits excellent viscous properties. In addition, the formed lubricating film is relatively thick, and its lubricating performance and time are both improved, thereby effectively reducing the energy consumption in the grinding process. The lower grinding zone temperature enables the formation of lubricating film with better lubricity in the grinding contact area, which reduces the energy consumption during the grinding process and achieves the best lubricating effect. Meanwhile, lower grinding temperature and oil film characteristics reduce the occurrence of cracking and evaporation of oil film due to high temperature and reduced the probability for local zone to be under the dry friction state within a period of short time. Simultaneously, the stability of the oil film and its lubricating effect are more excellent, there reducing the grinding force and heat input.

(4) The initial temperature of the cooling liquid (− 5 °C), which is carried by cryogenic air under CNMQL, is lower than that carried by room temperature air (25 °C) under NMQL. In addition, the average initial volume of the vaporization core under CNMQL is smaller. When the volume of the vaporization core increases, more energy is needed. Given the same specific heat of the cooling liquid, the temperature difference Δt between the evaporation latent heat stage to the evaporation temperature under CNMQL is higher than that of NMQL. With the decrease in temperature, the liquid molecules will have reduced kinetic energy, and the difference between the gas and liquid phase will increase. The vaporization energy absorbed by the liquid from outside will be higher in the two processes of boiling heat transfer. The total heat exchange of CNMQL from the grinding zone is higher than that of NMQL; it also achieved better comprehensive heat transfer effect than NMQL.

(5) Clear and smooth grinding pipelines, as well as slight plastic deformation and material adhesion, are present on the workpiece surface under CNMQ condition; however, no plows are detected. Thus, a small barrier, which hinders flow and spreading effect of the lubricating liquid along the pipelines to some extent, is present. Meanwhile, in the process of material removal, the bottom surface of the debris gradually curls up and presents high and low ripple ravines, which increases the adsorption area of the coolants. The surface geometry characteristics of the workpiece and grinding debris significantly increased the spreading effect and dynamic heat transfer area of coolant. Thus, more coolants can carry away heat from the grinding zone through the boiling heat transfer, thereby achieving the cooling and heat exchanging function better.

(6) To sum up, CNMQL combined the advantages of the two processing methods, namely, CA and NMQL, and achieved excellent grinding performance, as well as better cooling and lubricating effect. Moreover, CNMQL had the advantages of low cost and green and environmental friendly properties; thus, it can be used in the machine field.

Acknowledgments This research was financially supported by the following foundation items: The National Natural Science Foundation of China (51575290), Major Research Project of Shandong Province (2017GGX30135), and Shandong Provincial Natural Science Foundation, China (ZR2017PEE002 and ZR2017PEE011).

References

1. Xu X, Malkin S (2001) Comparison of methods to measure grinding temperatures. J Manuf Sci Eng 123(2):191–195
2. Zhang YB, Li CH, Jia DZ, Li BK, Wang YG, Yang M, Hou YL, Zhang XW (2016) Experimental study on the effect of nanoparticle concentration on the lubricating property of nanofluids for MQL grinding of Ni-based alloy. J Mater Process Technol 232:100–115
3. Guo SM, Li CH, Zhang YB, Wang YG, Li BK, Yang M, Zhang XP, Liu GT (2017) Experimental evaluation of the lubrication performance of mixtures of castor oil with other vegetable oils in MQL grinding of nickel-based alloy. J Cleaner Prod 140:1060–1076
4. Wang YG, Li CH, Zhang YB, Li BK, Yang M, Zhang XP, Guo SM, Liu GT, Zhai MG (2017) Comparative evaluation of the lubricating properties of vegetable-oil-based nanofluids between frictional test and grinding experiment. J Manuf Process 26:94–104
5. Ding WF, Zhang LH, Li Z, Zhu YJ, Su HH, Xu JH (2017) Review on grinding-induced residual stresses in metallic materials. Int J Adv Manuf Technol 88:2939–2968
6. Zhang YB, Li CH, Jia DZ, Zhang DK, Zhang XW (2015) Experimental evaluation of the lubrication performance of MoS_2/CNT nanofluid for minimal quantity lubrication in Ni-based alloy grinding. Int J Mach Tools Manuf 99:19–33
7. Xi XX, Ding WF, Li ZH, Xu JH (2017) High speed grinding of particulate reinforced titanium matrix composites using a monolayer brazed cubic boron nitride wheel. Int J Adv Manuf Technol 90:1529–1538
8. Li ZH, Ding WF, Liu CJ, Su HH (2017) Prediction of grinding temperature of PTMCs based on the varied coefficients of friction in conventional-speed and high-speed surface grinding. Int J Adv Manuf Technol 90:2335–2344
9. WD Hewson, GK Gerow (1999) High performance metal working oil: U.S. Patent 5958849. 9–28
10. Sadeghi MH, Haddad MJ, Tawakoli T, Emami M (2009) Minimal quantity lubrication–MQL in grinding of Ti–6Al–4V titanium alloy. Int J Adv Manuf Technol 44(5–6):487–500

11. Li CH (2018) Theory and key technology of nanofluid minimum quantity grinding. Science Press, Beijing, pp 125–187
12. Guo SM, Li CH, Zhang YB, Yang M, Jia DZ, Zhang XP, Liu GT, Li RZ, Bing ZR, Ji HJ (2018) Analysis of volume ratio of castor/soybean oil mixture on minimum quantity lubrication grinding performance and microstructure evaluation by fractal dimension. Ind Crop Prod 111:494–505
13. Yang M, Li CH, Zhang YB, Wang YG, Li BK, Jia DZ, Hou YL, Li RZ (2017) Research on microscale skull grinding temperature field under different cooling conditions. Appl Therm Eng 126:525–537
14. Luo T, Wei X, Huang X (2014) Tribological properties of Al2O3 nanoparticles as lubricating oil additives. Ceram Int 40(5):7143–7149
15. Mao C, Tang X, Zou H (2012) Investigation of grinding characteristic using nanofluid minimum quantity lubrication. Int J Precis Eng Manuf 13(10):1745–1752
16. Mao C, Zou HF, Huang XM, Zhang, JA, Zhou ZX (2013) The influence of spraying parameters on grinding performance for nanofluids minimum quantity lubrication. International Journal of Advanced Manufacturing Technology 64:1791–1799
17. Zhang YB, Li CH, Jia DZ, Zhang DK, Zhang XW (2015) Experimental evaluation of MoS2 nanoparticles in jet MQL grinding with different types of vegetable oil as base oil. J Clean Prod 87:930–940
18. Anuj KS, Rabesh KS, Amit RD, Arun KT (2016) Characterization and experimental investigation of Al2O3 nanoparticle based cutting fluid in turning of AISI 1040 steel under minimum quantity lubrication (MQL). MaterToday Proc 3(6):1899–1906
19. Lee PH, Nam JS, Li C (2012) An experimental study on micro-grinding process with nanofluid minimum quantity lubrication (MQL). Int J Precis Eng Manuf 13(3):331–338
20. Hadad MJ, Tawakoli T, Sadeghi MH, Sadeghi B (2012) Temperature and energy partition in minimum quantity lubrication–MQL grinding process. Int. J. Mach. Tools Manuf 54–55(3):10–17
21. Setti D, Sinha MK, Ghosh S et al (2014) An investigation into the application of Al_2O_3nanofluid–based minimum quantity lubrication technique for grinding of Ti–6Al–4V. Int J PrecisTechnol 4 (3–4):268–279
22. Su Y, Gong L, Li B, Liu Z, Chen D (2015) Performance evaluation of nanofluid mql with vegetable–based oil and ester oil as base fluids in turning. International Journal of Advanced Manufacturing Technology 1–7
23. Shane Y. Hong (2005) Investigation of liguid nitrogen lubrication effect in cryogenic machining. World Tribology Congress III 1:801–802
24. Manimaran G, Kumar MP, Venkatasamy R (2013) Influence of cryogenic cooling on surface grinding of stainless steel 316. Cryogenics 59:76–83
25. Ravi S, Kumar MP (2012) Experimental investigation of cryogenic cooling in milling of AISI D3 tool steel. Mater Manuf Process 27:1017–1021
26. Jawahir S, Xia T, Kaynak Y, Arvin C (2016) Cryogenic cooling-induced process performance and surface integrity in drilling CFRP composite mateial. Int J Adv Manuf Technol 82:605–616
27. Paul S, Chattopadhyay AB (1995) Effects of cryogenic cooling by liquid nitrogen jet on forces, temperature and surface residual stresses in grinding steels. Cryogenics 35(8):515–523
28. Schoop J, Effgen M, Balk TJ, Jawahir IS (2013) The effects of depth of cut and pre–cooling on surface porosity in cryogenic machining of porous tungsten. Procedia CIRP 8:357–362
29. Su Y, He N, Li L (2010) Cooling and lubricating performance of cryogenic minimum quantity lubrication method in high speed turning. Lubr Eng 35(9):52–55
30. Li XL (2004) Research on high–speed milling technology of titanium alloy based on LN_2 and MQL technology. Nanjing University of Aeronautics and Astronautics
31. He AD, Ye BY, Wang ZY (2014) Experimental effect of cryogenic MQL cutting 304 stainless steel. Key Eng Mater 621:3–8
32. Wang YF, Huang Y, Huang Z, Yi L (2009) Belt grinding of TC4 based on the technology of cryogenic mist jet combined MQL. Key Eng Mater 416:8–12
33. Wang YG, Li CH, Zhang YB, Yang M, Zhang XP, Zhang NQ, Dai JJ (2017) Experimental evaluation on tribological performance of the wheel/workpiece interface in MQL grinding with different concentrations of Al_2O_3 nanofluids. J Clean Prod 142(4:3571–3583
34. Demas NG, Timofeeva EV, Routbort JL (2012) Tribological effects of BN and MoS_2 nanoparticles added to polyalphaolefin oil in piston skirt/cylinder liner tests. Tribol Lett 47(1):91–102
35. Li BM, Zhao B (2003) Modern grinding technology. China Machine Press, Beijing
36. Shen B, Shih AJ, Xiao G (2011) A heat transfer model based on finite difference method for grinding. Journal of Manufacturing Science & Engineering 133(3):255–267
37. Zhang DK, Li CH, Zhang YB, Jia DZ, Zhang XW (2015) Experimental research on the energy ratio coefficient and specific grinding energy in nanoparticle jet MQL grinding. Int J Adv Manuf Technol 78(5–8):1275–1288
38. Zhao YX (1994) Experimental and theoretical research on the mechanism of boiling heat transfer in cold flow nuclear state. Shanghai institute of mechanics, Shanghai polytechnic university
39. Mao C, Zou HF, Huang Y, Li Y, Zhou Z (2014) Research on heat transfer mechanism in grinding zone for MQL surface grinding. China Mech Eng 25(6):826–831
40. Mao C, Tang XJ, Zou HF, Zhou ZX, Yin WF (2012) Experimental investigation of surface quality for minimum quantity oil-water lubrication grinding. Int J Adv Manuf Technol 59(1):93–100
41. Lin ZH (2003) Gas-liquid two-phase flow and boiling heat transfer. Xian Jiaotong University Press
42. Lu ZQ (2002) Two-phase flow and boiling heat transfer. Tsinghua University Press
43. Xin MD (1987) Boiling heat transfer and its reinforcement. Chongqing University Press
44. Yang SM, Tao WQ (2006) Beijing: Higher Education Press
45. Maruda RW, Krolczyk GM, Feldshtein E (2016) A study on droplets sizes, their distribution and heat exchange for minimum quantity cooling lubrication (MQCL). Int J Mach Tool Manu 100:81–92
46. Mao C, Zou H, Huang Y (2013) Analysis of heat transfer coefficient on workpiece surface during minimum quantity lubricant grinding. Int J Adv Manuf Technol 66(1–4):363–370
47. Mei GH, Meng HJ, Wu RY, Ci Y, Xie Z (2004) Analysis of spray cooling heat transfer coefficient on high temperature surface. Energy Metall Ind 23(6):18–22
48. Deb S, Yao SC (1989) Analysis on film boiling heat transfer of impacting spray. Heat Mass Transf 32:2099–2112
49. Chu MQ, Yu BM (2009) Fractal analysis of boiling heat exchange. Mech Progress 03:259–272
50. Bang IC, Chang SH (2005) Boiling heat transfer performance and phenomena of Al2O3-water nanofluids form a plain surface in a pool. Int J Heat Mass Transf. International Journal of Heat & Mass Transfer 48:2407–2419

Publisher's Note